

Instabilities leading to vortex lattice formation in rotating Bose-Einstein condensates

N. G. Parker¹, R. M. W. van Bijnen^{1,2}, and A. M. Martin¹

¹ *School of Physics, University of Melbourne, Parkville, Victoria 3010, Australia and*

² *Eindhoven University of Technology, PO Box 513, 5600 MB Eindhoven, The Netherlands*

(Dated: December 17, 2021)

We present a comprehensive theoretical study of vortex lattice formation in atomic Bose-Einstein condensates confined by a rotating elliptical trap. We consider rotating solutions of the classical hydrodynamic equations, their response to perturbations, as well as time-dependent simulations. We discriminate three distinct, experimentally testable, regimes of instability: *ripple*, *interbranch*, and *catastrophic*. Under symmetry-breaking perturbations these instabilities lead to lattice formation even at zero temperature. While our results are consistent with previous theoretical and experimental results, they shed new light on lattice formation.

PACS numbers: 03.75.Kk, 34.20.Cf, 47.20.-k

Vortex lattices are a striking manifestation of superfluidity in rotating systems. In recent years such states have been generated in atomic Bose-Einstein condensates (BECs) via rotation in an elliptical harmonic trap [1, 2, 3], in analogy to the classic rotating bucket experiment in superfluid Helium [4]. Vortex lattices form for trap rotation frequencies Ω in the region of $\Omega \sim 0.7\omega_{\perp}$, where ω_{\perp} is the mean harmonic trap frequency in the rotating plane. Although a vortex lattice is thermodynamically favourable for much lower rotation frequencies, the *instabilities* necessary to seed vortex lattice formation are only present in the region of $\Omega \sim 0.7\omega_{\perp}$. Such instabilities have been predicted by hydrodynamic studies of condensate solutions in the rotating frame [5] and the dynamical perturbations of these states [6], and have also been analysed in dipolar BECs [7]. Although numerical simulations of the Gross-Pitaevskii equation have also observed vortex lattice formation in this region [8, 9, 10, 11, 12, 13], the results are mixed: for $\Omega \lesssim 0.7\omega_{\perp}$, Refs. [8, 9, 10] require thermal effects to enable vortex nucleation, while Ref. [11] does not; for $\Omega \gtrsim 0.7\omega_{\perp}$, Refs. [8, 11, 12, 13] observe a shape instability before nucleating vortices even in the absence of thermal effects. This is consistent with experiments [3, 14] which indicate that lattice formation is temperature-independent. Breaking the rotational symmetry of such simulations has been shown to be crucial to enable realistic nucleation of vortices [12].

In this paper we present a thorough investigation of the instabilities leading to vortex lattice formation in elliptical traps in the regime $\Omega \leq \omega_{\perp}$. We primarily consider the cases when the trap ellipticity or rotation frequency is introduced adiabatically, for which it is appropriate to transform to the rotating frame. In order to probe the condensate instabilities we consider the rotating frame condensate solutions within the classical hydrodynamic regime and the response of these states to dynamical perturbations. Furthermore we perform time-dependent (TD) condensate simulations to test our results, and probe the fate of the unstable condensate.

In the experiments [1, 3] the harmonic trap confining the BEC is transformed radially into an ellipse and ro-

tated about the z -axis. In the limit of zero temperature, the condensate can be approximated by a mean-field ‘wavefunction’ ψ , which can be expressed as $\psi = \sqrt{\rho}e^{i\phi}$, where ρ and ϕ are the condensate density and phase. In the frame rotating at Ω , the density ρ and fluid velocity $\mathbf{v} = (\hbar/m)\nabla\phi$ [15] satisfy the hydrodynamic equations,

$$\frac{\partial\rho}{\partial t} + \nabla \cdot [\rho(\mathbf{v} - \boldsymbol{\Omega} \times \mathbf{r})] = 0, \quad (1)$$

$$m\frac{\partial\mathbf{v}}{\partial t} + \nabla \left(\frac{1}{2}m\mathbf{v} \cdot \mathbf{v} + \frac{1}{2}m(\omega_x^2 x^2 + \omega_y^2 y^2 + \omega_z^2 z^2) + \rho g - \frac{\hbar^2}{2m} \frac{\nabla^2 \sqrt{\rho}}{\sqrt{\rho}} - m\mathbf{v} \cdot [\boldsymbol{\Omega} \times \mathbf{r}] \right) = 0. \quad (2)$$

Here m is the atomic mass and $g = 4\pi\hbar^2 a/m$ is the interaction coefficient, where a is the s -wave scattering length (in this work $g > 0$). The harmonic trap is defined by the frequencies ω_x , ω_y and ω_z . When the trap is elliptical in the radial plane we can write the x, y frequencies as $\omega_x = \sqrt{1-\epsilon}\omega_{\perp}$ and $\omega_y = \sqrt{1+\epsilon}\omega_{\perp}$, where ϵ characterises the trap ellipticity, and $\omega_{\perp}^2 = (\omega_x^2 + \omega_y^2)/2$.

Following the approach by Recati *et al.* [5], we employ the Thomas-Fermi (TF) approximation by neglecting the $(\nabla^2 \sqrt{\rho}/\sqrt{\rho})$ term in Eq. (2). Furthermore we assume an irrotational quadrupolar velocity field [16],

$$\mathbf{v} = \alpha \nabla(xy), \quad (3)$$

where α is the velocity field amplitude. Substituting this into Eq. (2) and setting $\partial\rho/\partial t = \partial\mathbf{v}/\partial t = 0$, we obtain stationary density solutions of the form,

$$\rho_0 = \frac{1}{g} \left[\mu - \frac{1}{2}m(\tilde{\omega}_x^2 x^2 + \tilde{\omega}_y^2 y^2 + \omega_z^2 z^2) \right], \quad (4)$$

in the region where the chemical potential $\mu \geq m(\tilde{\omega}_x^2 x^2 + \tilde{\omega}_y^2 y^2 + \omega_z^2 z^2)/2$, and $\rho_0 = 0$ elsewhere. The effect of the rotation is to give *effective* trap frequencies, which satisfy,

$$\tilde{\omega}_x^2 = [(1-\epsilon) + \alpha^2 - 2\alpha\Omega] \omega_{\perp}^2 \quad (5)$$

$$\tilde{\omega}_y^2 = [(1+\epsilon) + \alpha^2 + 2\alpha\Omega] \omega_{\perp}^2, \quad (6)$$

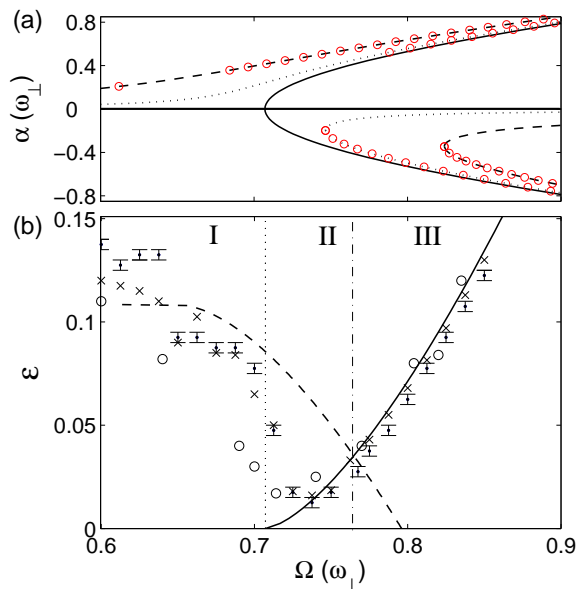


FIG. 1: (a) Velocity field amplitude α of the stationary solutions of Eq. (7) as a function of rotation frequency Ω for $\epsilon = 0$ (solid line), 0.02 (dotted line) and 0.1 (dashed line). Regions of dynamical instability for $\epsilon = 0.02$ and 0.1 are shown (circles). (b) Phase diagram of ϵ versus Ω . Plotted are the bifurcation point $\Omega_{\text{bif}}(\epsilon)$ (solid line) from Eq. (7), the onset of dynamical instability $\Omega_{\text{ins}}(\epsilon)$ from Eq. (8) (dashed line), and experimental data of Hodby *et al.* [3] (circles). Furthermore, time-dependent simulations of Eqs. (1) and (2) show the critical ellipticities beyond which the condensate deviates from an elliptical shape $\epsilon_{\text{cr}}^{\text{dev}}$ (crosses) and beyond which lattice formation ultimately occurs $\epsilon_{\text{cr}}^{\text{inst}}$ (points with error bars). The bifurcation point for $\epsilon = 0$ (dotted line) and crossing frequency Ω_X (dot-dashed line) at which $\Omega_{\text{bif}}(\epsilon) = \Omega_{\text{ins}}(\epsilon)$ are indicated. We assume a condensate with $\mu = 10\hbar\omega_{\perp}$.

where α determines the ellipticity of the BEC density [5]. Plugging Eq. (4) into Eq. (1) we obtain [5],

$$\tilde{\omega}_x^2(\alpha + \Omega) + \tilde{\omega}_y^2(\alpha - \Omega) = 0, \quad (7)$$

which specifies the stationary condensate solutions in the frame rotating at Ω (in the TF regime).

Figure 1(a) shows the stationary solutions in Ω - α space for various values of trap ellipticity ϵ . In the limit of $\epsilon = 0$ (solid line) a non-rotating ($\alpha = 0$) solution occurs for all Ω , with two additional solutions bifurcating from the $\alpha = 0$ axis at $\Omega_{\text{bif}}^0 = \omega_{\perp}/\sqrt{2}$. For finite ϵ (dotted and dashed lines), the $\alpha = 0$ solution disappears and the plot consists of two distinct branches. The *upper* branch (positive α) is single-valued and exists for all Ω , while the *lower* branch (negative α) is double-valued and exists only when Ω is greater than the bifurcation frequency $\Omega_{\text{bif}}(\epsilon)$. As ϵ is increased from zero, the branches move away from the $\alpha = 0$ axis, as can be seen in Fig. 1(a). Furthermore the bifurcation point of the lower branch $\Omega_{\text{bif}}(\epsilon)$ shifts to higher rotation frequencies, as shown in Fig. 1(b) (solid line). The branch diagrams, which have been probed experimentally [2], are key to understanding

the response of the system to the adiabatic introduction of trap ellipticity ϵ or rotation frequency Ω . Before any rotation/ellipticity is applied the BEC has $\alpha = 0$. When Ω is increased adiabatically (for fixed ϵ), the BEC follows the upper branch, with increasing α and ellipticity in the density profile. When ϵ is introduced adiabatically (for fixed Ω), the BEC can follow two routes, depending on the value of Ω relative to the bifurcation point Ω_{bif}^0 (dotted line in Fig. 1(b)). For $\Omega < \Omega_{\text{bif}}^0$, the lower branch is nonexistent and the BEC follows the upper branch to increasing values of α . For $\Omega > \Omega_{\text{bif}}^0$, the lower branch moves from $\alpha = 0$ to negative α , and the BEC follows this route. However, as ϵ is increased, the edge of the lower branch $\Omega_{\text{bif}}(\epsilon)$ shifts to higher frequencies, and when $\Omega_{\text{bif}}(\epsilon) > \Omega$ the lower branch no longer exists. In this manner, the evolution of the branches can induce instability, and has been linked to lattice formation [2].

The stationary solutions of Eq. (7) are not necessarily *stable* solutions. To investigate their stability we follow the approach of Sinha and Castin [6] by considering small perturbations $\delta\rho$ and $\delta\phi$ of stationary solutions of density ρ_0 and phase ϕ_0 . Taking variational derivatives of Eqs. (1) and (2) we obtain the time evolution equations,

$$\frac{\partial}{\partial t} \begin{bmatrix} \delta\phi \\ \delta\rho \end{bmatrix} = - \begin{bmatrix} \mathbf{v}_{\mathbf{c}} \cdot \nabla & g/m \\ \nabla \cdot (\rho_0 \nabla) & \mathbf{v}_{\mathbf{c}} \cdot \nabla \end{bmatrix} \begin{bmatrix} \delta\phi \\ \delta\rho \end{bmatrix} \quad (8)$$

where $\mathbf{v}_{\mathbf{c}} = \mathbf{v} - \Omega \times \mathbf{r}$ is the velocity field in the rotating frame. The eigenfunctions of Eq.(8) grow in time as $e^{\lambda t}$, where λ is the corresponding eigenvalue. Solutions are unstable when there exist one or more eigenfunctions for which λ contains a positive real part. Such unstable solutions are thought to seed vortex lattice formation [6].

Using a polynomial ansatz for the perturbations, this method predicts a region of dynamical instability when Ω exceeds a critical value $\Omega_{\text{ins}}(\epsilon)$ [6], as indicated in Fig. 1(a) (circles). The unstable modes have lengthscales of the order of the condensate size, much greater than the healing length $\xi = \hbar/\sqrt{m n_0 g}$ which characterises the vortex size. In the limit of $\epsilon = 0$, $\Omega_{\text{ins}} \approx 0.78\omega_{\perp}$. As ϵ is increased, $\Omega_{\text{ins}}(\epsilon)$ is reduced (dashed line in Fig. 1(b)). Note that the outlying point in Fig. 1(a) for $\epsilon = 0.1$ (dashed line) at $\Omega \approx 0.61\omega_{\perp}$ is not considered to be in the region of instability due to its narrow width and comparatively small eigenvalues [18]. Note that, for the parameter space of interest, on the lower branch the solution closest to the $\alpha = 0$ axis is never dynamically unstable. A key rotation frequency in our work is Ω_X , which is the crossing point of $\Omega_{\text{bif}}(\epsilon)$ and $\Omega_{\text{ins}}(\epsilon)$, and has the value $\Omega_X \approx 0.765\omega_{\perp}$ (dot-dashed line in Fig. 1(b)).

Based on the stationary solutions of Eq. (7) and the dynamical instability of Eq. (8) we can predict the stability of a BEC following the adiabatic introduction of Ω or ϵ . However, to determine how the instability *manifests* itself and whether it leads to lattice formation we perform TD simulations of Eqs. (1) and (2) in the laboratory frame. This is equivalent to solving the Gross-Pitaevskii equation [12]. Following previous approaches [9, 10, 11, 12], and noting that the solutions of Eqs. (7) and (8) are

independent of z [19], we consider a 2D system. The initial state is found by imaginary-time propagation. Then, in real time, either ϵ is ramped up linearly at a rate of $d\epsilon/dt = 10^{-4}\omega_{\perp}$ (for fixed Ω), or Ω is ramped up linearly at a rate $d\Omega/dt = 10^{-2}\omega_{\perp}^2$ (for fixed ϵ). We monitor the evolution of α by fitting the velocity field in a central region $[3 \times 3]\mu\text{m}$ to the form of Eq. (3).

In such ‘idealised’ simulations the trap and BEC can maintain a two-fold rotational symmetry to unrealistic levels. This strongly inhibits vortex nucleation since the vortices must enter in pairs rather than individually. Symmetry-breaking, rather than thermal effects, has been shown to be crucial in simulating lattice formation [12]. Indeed, Eq. (8) predicts that only odd modes of the system are dynamically unstable. Previous studies [8, 10] have broken this symmetry through the introduction of thermal ‘noise’. To overcome this problem we shift the trap by half a healing length before running in real-time, thereby allowing excitation of odd modes [17].

We first consider the adiabatic increase of trap ellipticity ϵ for fixed Ω . We discriminate three cases of instability, which each occur in distinct frequency regimes, as indicated in Fig. 1(b): (I) ripple instability, (II) interbranch instability, and (III) catastrophic instability. We will discuss each in turn.

I Ripple instability, $\Omega < \omega_{\perp}/\sqrt{2}$. The case for $\Omega = 0.7\omega_{\perp}$ is shown in Fig. 2I(a). The velocity field amplitude α (dots) follows the upper branch of the rotating solutions (solid line), for which the condensate axes rotate in phase with the trap axes, as noted experimentally [2, 3]. The upper branch is always a solution, and, as ϵ is increased, the condensate moves along the branch to higher α . However, when the ellipticity exceeds a critical value ϵ_{cr} (corresponding to when $\Omega > \Omega_{\text{inst}}$) the solution becomes dynamically unstable, according to Eq. (8). For the example in Fig. 2I(a), $\epsilon_{\text{cr}} \approx 0.09$ (dashed line). Subsequently α (dots) deviates from the rotating solutions of Eq. (7) (solid lines), consistent with the onset of dynamical instability. For low ϵ , α (dots) features small oscillations due to the centre-of-mass motion caused by the initial offset of the condensate.

At a critical ellipticity $\epsilon_{\text{cr}}^{\text{dev}}$ low density ripples form on the condensate edge (Fig. 2I(b)), each on the scale of the healing length and featuring a phase singularity (‘ghost’ vortices [8, 9, 10]). These ripples grow in amplitude as ϵ is increased. If ϵ becomes fixed when the ripples have very low amplitude they do not grow over the timescales considered. However, once ϵ exceeds a second critical value $\epsilon_{\text{cr}}^{\text{ins}}$ (corresponding to when the ripples have amplitude of order of $10\%n_0$), the dynamical instability of Eq. (8) is triggered by the ripples. This instability generates largescale shape oscillations (Fig. 2I(c)), disrupting the condensate, and enabling ‘ghost’ vortices to nucleate into the condensate, which slowly crystallise into a lattice (Fig. 2I(d)) [12]. Once $\epsilon_{\text{cr}}^{\text{ins}}$ is reached, lattice formation occurs independently of whether ϵ becomes fixed or continuously increased. Since the ripples that trigger the dynamical instability originate in the non-TF tails of

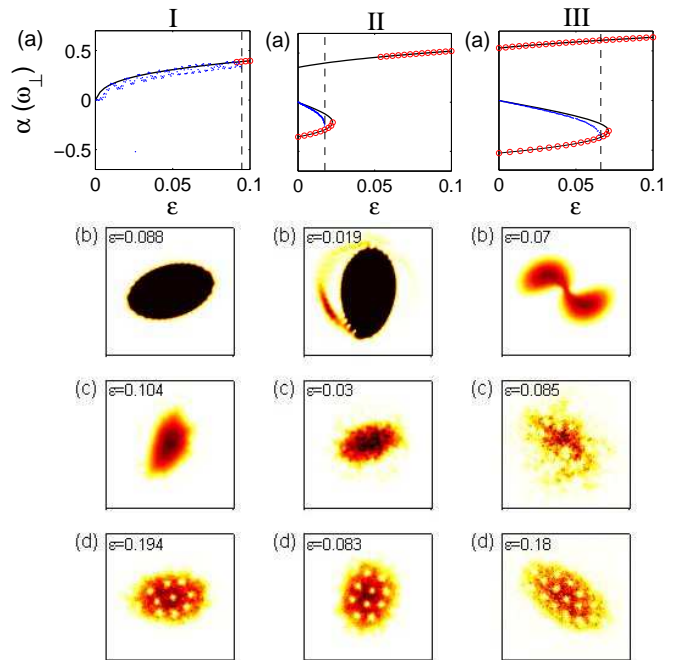


FIG. 2: Dynamics under a continuous increase of ϵ (at a rate of $d\epsilon/dt = 10^{-4}\omega_{\perp}$) for I. Ripple instability ($\Omega/\omega_{\perp} = 0.7$), II. Interbranch instability ($\Omega/\omega_{\perp} = 0.75$), and III. Catastrophic instability ($\Omega/\omega_{\perp} = 0.8$). (a) Velocity field amplitude α versus ϵ according to Eq. (7) (solid lines) and TD simulations of Eqs. (1) and (2) (dots). In the latter case, α is derived by fitting the velocity field to Eq. (3). To the right of the dashed line this is no longer a valid fit (the standard deviation of the fit becomes of the order of α). The regions of dynamical instability are indicated (circles). Density snapshots corresponding to (b) the onset of instability, (c) disrupted state seeded by the instability, and (d) a vortex lattice. Once the instability point is reached, the dynamics are qualitatively similar whether ϵ is continuously increased or becomes fixed. Dark/light regions represent high/low density. Each box represents a region $(12 \times 12)\mu\text{m}$ (the simulation box is much greater than this). In I(b) and II(b) the density scale is limited to $0.1\%n_0$ to highlight low density features.

the BEC, they cannot be explained by the TF analytics of Eqs. (3) - (8), and a higher-order (non-TF) approach would be required to explain their origin.

Surface ripples have been observed experimentally to precede vortex nucleation at this rotation frequency [3]. The gradual growth of the ripples leads to a *slow* injection of energy/angular momentum into the system, as has been observed in previous studies within this frequency regime [8, 11]. Note that according to Eq. (8) the dynamical instability on the upper branch couples to odd modes only. If the symmetry is preserved we do not expect the instability to develop [8, 9, 10].

II Interbranch instability, $\omega_{\perp}/\sqrt{2} < \Omega < \Omega_X$. The case for $\Omega = 0.75\omega_{\perp}$ is shown in Fig. 2II(a). Since $\Omega > \omega_{\perp}/\sqrt{2}$, α (dots) initially follows the lower branch solutions, where we observe that the BEC and trap axes

are $\pi/2$ out of phase. As ϵ is increased a point is reached when $\Omega < \Omega_{\text{bif}}(\epsilon)$. Here the lower branch is no longer a solution of Eq. (7). For the example shown, this occurs for $\epsilon \approx 0.02$ (dashed line in Fig. 2II(a)). Due to the non-TF nature of the numerical solutions of Eqs. (1) and (2), α does not perfectly fit the branch solutions of Eq. (7).

When α (dots) reaches the cusp of the lower branch it deviates non-adiabatically, as observed experimentally [2]. Since $\Omega < \Omega_X$, the upper branch is dynamically stable at this ellipticity. The condensate tries to transform to the upper branch, but without dissipation it cannot relax to this state. Instead α (dots) oscillates between positive and negative values, and the condensate density undergoes quadrupolar shape oscillations between an almost circular and highly elliptical shape. If ϵ becomes fixed close to this critical ellipticity, the quadrupolar shape oscillations are stable. However, if ϵ is increased further, the shape oscillations destabilise, with the condensate shedding low density material at its extrema in a spiral pattern (Fig. 2II(b)). This situation is closely analogous to when the rotation/ellipticity is suddenly turned on, with the fate of the condensate being qualitatively similar [12, 13]. The growth of the ejected material gradually destabilises the condensate (Fig. 2II(c)), leading to vortex nucleation and ultimately a lattice (Fig. 2II(c)). This is fully consistent with the observations in [2].

III Catastrophic instability, $\Omega > \Omega_X$. The case for $\Omega = 0.8\omega_\perp$ is shown in Fig. 2III(a). Again α (dotted line) follows the lower branch, which ceases to be a solution at some critical ϵ (dashed line). However, since $\Omega > \Omega_X$, the upper branch is dynamically unstable at this point, and *no* stable solutions exist. The BEC undergoes a quick and catastrophic instability, with α (dots) deviating rapidly from the rotating solutions of Eq. (7). The BEC density profile becomes strongly contorted into a spiral shape (Fig. 2III(b)). The arms of the spiral collapse inwards and trap phase singularities to form vortices. Energy and angular momentum are very rapidly injected into the BEC (in contrast to the gradual ripple and interbranch instabilities), as observed in [8, 11] for this frequency regime. The BEC becomes highly excited and turbulent (Fig. 2III(c)), with structure on length-scales less than the healing length. Although we observe this state to ultimately settle into a lattice (Fig. 2II(c)), one may question the validity of our zero-temperature condensate simulations for such a ‘heated’ state. Indeed, for $\Omega \gtrsim 0.78\omega_\perp$, turbulent states, rather than vortex lattices, were observed experimentally in [1].

In the TD simulations we have measured two distinct critical ellipticities: $\epsilon_{\text{cr}}^{\text{dev}}$ (crosses in Fig. 1(b)) is when, for a continuously increasing ϵ , we observe the density to deviate from a smooth ellipse (on the level of $0.1\%n_0$); $\epsilon_{\text{cr}}^{\text{inst}}$ (points with error bars in Fig. 1(b)) is when, for ϵ ramped up to some final value, instability and lattice formation ultimately occur. In regime I, typically $\epsilon_{\text{cr}}^{\text{dev}} \leq \epsilon_{\text{cr}}^{\text{inst}}$ since surface ripples are generated which are stable for a nar-

row range of ϵ , above which they induce instability and lattice formation. In regimes II and III, $\epsilon_{\text{cr}}^{\text{dev}} \approx \epsilon_{\text{cr}}^{\text{inst}}$, indicating the relatively sudden onset of this instability once the density deviates from a smooth ellipse.

According to the TD simulations, the region above the points in Fig. 1(b) is unstable, leading to lattice formation. The prediction of Eq. (8) (dashed line) gives reasonable agreement with the TD results in region I, while Eq. (7) gives excellent agreement in region III. Also plotted in Fig. 1(b) are the experimental results of Hodby *et al.* [3] (circles). The TD results give good agreement with the experimental data throughout, with the agreement being particularly good in region III.

So far we have considered the adiabatic introduction of ellipticity for fixed Ω . However, the results in Fig. 1(b) also apply to the case when Ω is introduced adiabatically for fixed ϵ . Here the condensate always follows the upper branch and so is only prone to the ripple instability when the upper branch solution becomes dynamically unstable. According to Eq. (8) dynamical instability occurs when $\Omega > \Omega_{\text{inst}}(\epsilon)$ (dashed line in Fig. 1(b)). In [2], for $\epsilon = 0.025$, vortex lattice formation was observed to occur when $\Omega \gtrsim 0.75\omega_\perp$, which agrees well with our TD simulations and Fig. 1(b).

Equations (7) and (8) are valid in the TF limit of $\mu/\hbar\omega_\perp \gg 1$. For the TD simulations of Eqs. (1) and (2), which do not make this assumption, we have employed an intermediate value of $\mu/\hbar\omega_\perp = 10$, but have tested other values. For less (more) Thomas-Fermi-like condensates, the TD results in Fig. 1(b) shift downwards (upwards), deviating away from (towards) the TF predictions of Eqs. (7) and (8). In particular, as $\mu/\hbar\omega_\perp$ is increased, the TD values of α in Fig. 2 II-III(a) (dots) become closer to the branch solutions (solid lines).

We have shown that vortex lattice formation is inherently a two-dimensional and zero temperature effect. We have theoretically mapped out the condensate stability as a function of rotation frequency Ω and trap ellipticity ϵ , with our interpretation being consistent with previous experimental and theoretical results. Specifically, for fixed Ω and adiabatic introduction of ϵ we find three distinct regimes of instability - *ripple* ($\Omega < \omega_\perp/\sqrt{2}$), *interbranch* ($\omega_\perp/\sqrt{2} < \Omega < \Omega_X$) and *catastrophic* ($\Omega > \Omega_X$). Each instability manifests itself in a characteristic manner, which could be observed experimentally. Ultimately in each case the instability seeds vortex lattice formation. This formation process not only relies on the presence of an instability but is crucially dependent on the breaking of the two-fold rotational symmetry of the system, as inevitably occurs experimentally.

We acknowledge support from the ARC and the University of Melbourne. We thank Y. Castin, C. S. Adams and C. J. Foot for helpful comments, and C. J. Foot for the use of experimental data.

-
- [1] K. W. Madison, F. Chevy, W. Wohlleben, and J. Dalibard, Phys. Rev. Lett. **84**, 806 (2000).
- [2] K. W. Madison, F. Chevy, V. Bretin, and J. Dalibard, Phys. Rev. Lett. **86**, 4443 (2001).
- [3] E. Hodby *et al.*, Phys. Rev. Lett. **88**, 010405 (2002).
- [4] D. V. Osborn, Proc. Phys. Soc. A **63**, 909 (1950).
- [5] A. Recati, F. Zambelli and S. Stringari, Phys. Rev. Lett. **86**, 377 (2001).
- [6] S. Sinha and Y. Castin, Phys. Rev. Lett. **87**, 190402 (2001).
- [7] R. M. W. van Bijnen, D. H. J. O'Dell, N. G. Parker, and A. M. Martin, cond-mat/0602572 (2006).
- [8] C. Lobo, A. Sinatra, and Y. Castin, Phys. Rev. Lett. **92**, 020403 (2004)
- [9] M. Tsubota, K. Kasamatsu, and M. Ueda, Phys. Rev. A **65**, 023603 (2002); K. Kasamatsu, M. Tsubota, and M. Ueda, Phys. Rev. A **67**, 033610 (2003).
- [10] A. A. Penckwitt, R. J. Ballagh, and C. W. Gardiner, Phys. Rev. Lett. **89**, 260402 (2002)
- [11] E. Lundh, J.-P. Martikainen and K.-A. Suominen, Phys. Rev. A **67**, 063604 (2003).
- [12] N. G. Parker and C. S. Adams, Phys. Rev. Lett. **95**, 145301 (2005).
- [13] N. G. Parker and C. S. Adams, J. Phys. B **39**, 43 (2006).
- [14] J. R. Abo-Shaeer, C. Raman, and W. Ketterle, Phys. Rev. Lett. **88**, 070409 (2002).
- [15] This is the fluid velocity \mathbf{v} in the laboratory frame, expressed in rotating frame coordinates.
- [16] Y. Castin and R. Dum, Eur. Phys. J. D **7**, 399 (1999).
- [17] Over long times, symmetry can break intrinsically through the stimulated growth of numerical noise [12, 13].
- [18] Numerical simulations do not indicate any dynamical instability within these narrow, low eigenvalue regions.
- [19] As in [6] we find that the regions of instability according to Eq. (8) are independent of ω_z .